

Cascaded Multi-Scale Attention for Enhanced Multi-Scale Feature Extraction and Interaction with Low-Resolution Images

Xiangyong Lu^a, Masanori Suganuma^{a,b}, Takayuki Okatani^{a,b,**}

^aGraduate School of Information Sciences, Tohoku University, Japan

^bRIKEN Center for AIP, Japan

ABSTRACT

In real-world applications of image recognition tasks, such as human pose estimation, cameras often capture objects, like human bodies, at low resolutions. This scenario poses a challenge in extracting and leveraging multi-scale features, which is often essential for precise inference. To address this challenge, we propose a new attention mechanism, named cascaded multi-scale attention (CMSA), tailored for use in CNN-ViT hybrid architectures, to handle low-resolution inputs effectively. The design of CMSA enables the extraction and seamless integration of features across various scales without necessitating the downsampling of the input image or feature maps. This is achieved through a novel combination of grouped multi-head self-attention mechanisms with window-based local attention and cascaded fusion of multi-scale features over different scales. This architecture allows for the effective handling of features across different scales, enhancing the model's ability to perform tasks such as human pose estimation, head pose estimation, and more with low-resolution images. Our experimental results show that the proposed method outperforms existing state-of-the-art methods in these areas with fewer parameters, showcasing its potential for broad application in real-world scenarios where capturing high-resolution images is not feasible. Code is available at <https://github.com/xyongLu/CMSA>.

1. Introduction

In recent years, the application of deep learning for image recognition has significantly broadened its scope in the real world. At the forefront, there is the use under tougher conditions for image recognition. One of these is the application to low-resolution images. In this paper, we discuss how to maximize the estimation accuracy for several typical image recognition problems using images of a lower resolution than those primarily considered in previous studies, as illustrated in the left panel of Figure 1.

There are several scenarios where handling low-resolution images is necessary. One is when ideal image capture conditions are not achievable, resulting in objects not being adequately resolved in images. For instance, this can occur when

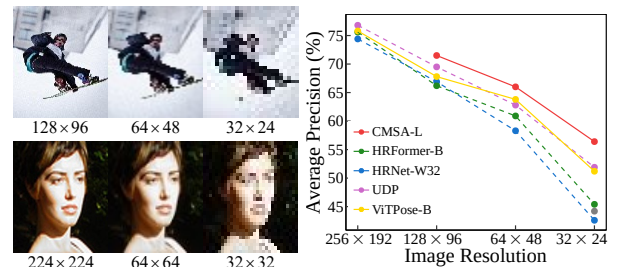


Fig. 1. Left: Estimating pose from low-resolution images. Left-Upper: human pose estimation from COCO2017. Left-Lower: head pose estimation from AFLW2000. Right: resolution-accuracy trade-off for human pose estimation evaluated on COCO 2017 val dataset.

trying to estimate specific information, such as the pose of a person located at a relative distance from a fixed camera, like a surveillance camera. Another scenario involves conducting image recognition on low-performance edge devices. Being able to make estimations from lower-resolution images could lead to

**Correspondence to: 6-3-09 Aoba, Aramaki-aza Aoba-ku, Sendai, 980-8579, Japan.

e-mail: okatani@vision.is.tohoku.ac.jp (Takayuki Okatani)

reductions in device costs and computational demands.

In this paper, we explore network architectures suitable for the above applications. Specifically, we build upon the recently evolved CNN-ViT hybrid models to design an architecture that can effectively handle low-resolution inputs. In particular, our goal is to perform multi-scale feature extraction from images and to facilitate appropriate interactions among these features.

Why do we aim to do this? First, multi-scale feature extraction combined with their interactions is an essential component for several tasks. The estimation of human poses mentioned earlier is a prime example of this necessity, as evidenced by previous studies (Cheng et al., 2020; Yuan et al., 2021b; Wang et al., 2022c). While the level of necessity may differ, this strategy is fundamentally beneficial across a broad spectrum of image recognition tasks, including, for example, fine-grained object recognition (Ibh et al., 2023) and biomedical image segmentation (Heidari et al., 2023).

Second, low resolution complicates the management of multi-scale features. The conventional approach generates multi-scale features through the downsampling of feature maps (Sun et al., 2019; Cheng et al., 2020; Yuan et al., 2021b; Yu et al., 2021). This method is effective when starting with high-resolution images. However, with low-resolution inputs, repeated downsampling quickly diminishes the resolution of feature maps to the point where additional downsampling results in a significant loss of information.

To address this challenge, we investigate methods to manage multi-scale feature maps without downsampling, enabling interactions between features of varying scales. Specifically, we first divide the multi-heads in Multi-Head Self-Attention (MHSA) into several groups, each of which processes features of a different scale. Then, instead of downsampling, we adopt the window-based self-attention mechanism from the Swin Transformer (Liu et al., 2021) to extract a different scale feature in each group. To facilitate effective interactions among features of different scales, we transfer a feature map from one group to another in an order from lower to higher scales. The transferred feature is utilized in the attention calculations of the subsequent group.

The approach to handling multi-scale features through grouping heads in the first part, and the cascading calculation structure in the latter part, are inspired by recent CNN-ViT hybrid models, SG-Former (Ren et al., 2023) and EfficientViT (Liu et al., 2023), respectively. It is important to note that these existing models, while aiming to address the high computational demands of the ViT architecture and improve the trade-off between performance and computation, were not designed with low-resolution images or the extraction of multi-scale features plus their interactions in mind.

We present experimental results across three distinct tasks: human pose estimation, head pose estimation, and image classification, all utilizing low-resolution image inputs. The results demonstrate that our proposed method achieves superior performance than existing state-of-the-art methods tailored for these individual tasks; see the right panel of Figure 1. It is also noted that our method needs fewer parameters than the existing methods.

2. Related work

2.1. Extraction and Use of Multi-Scale Features

Integrating features from multiple scales improves neural networks’ ability to deeply understand complex visual scenes. HRNet (Sun et al., 2019; Cheng et al., 2020) and HRFormer (Yuan et al., 2021b) fuse the multi-scale representations from multiple branches to effectively generate reliable high-resolution representations with strong position sensitivity. CrossViT (Chen et al., 2021) learns multi-scale feature representations for image recognition by a dual-branch transformer and merges them multiple times to complement each other. TopFormer (Zhang et al., 2022) produces scale-aware global features from tokens at various scales. P2T (Wu et al., 2022) and Shunted Transformer (Ren et al., 2022) improve upon PVT (Wang et al., 2021) by applying various downsampling rates for the keys and values across heads, rather than using identical spatial reduction for both. This allows each head to capture both coarse- and fine-grained details. SG-Former (Ren et al., 2023) aggregates tokens at multiple scales and performs attention mechanisms to extract global and fine-grained information for visual tasks. SMT (Lin et al., 2023b) captures diverse spatial features through multiple convolutions with different kernel sizes and conducts scale-aware aggregation to enhance information interaction. SBCFormer (Lu et al., 2024) achieves efficient global and local feature fusion by introducing a bi-branch CNN-ViT hybrid module. In existing methods, multi-scale representations are typically generated by downsampling the feature map, which can be problematic for low-resolution inputs, as it exacerbates the loss of detail. Our study mitigates this issue by enabling multi-scale feature extraction and interaction without the need for downsampling.

2.2. Dealing with Low-Resolution Images

Low-resolution images often lack clarity in fine textures, edges, and small details, presenting significant challenges in image analysis. Some studies tackle this issue by incorporating augmented inputs or utilizing additional knowledge from fully trained teacher models. DeriveNet (Singh et al., 2021) introduces a multi-resolution pyramid-based data augmentation technique to learn effective features from low-resolution images. NLSA (Mei et al., 2021) proposes a non-local sparse attention to explore long-range feature correlations in low-resolution images. CAL (Wang et al., 2022a) employs Gaussian offset weighting to account for displacements between coarse predictions and ground-truth positions in low-resolution images. FMD (Huang et al., 2022) proposes a feature distillation framework to transfer high-definition knowledge from a teach model for improved low-resolution object recognition. On the other hand, in order to reconstruct fine details from low-resolution images, recent Transformer-based approaches are gaining interest. ESRT (Lu et al., 2022) combines a CNN backbone with a Transformer backbone to recover a super-resolution image from its degraded low-resolution counterpart. ESSAformer (Zhang et al., 2023c) proposes an attention-embedded Transformer to enlarge the receptive field, allowing for better extraction of information from low-resolution

hyperspectral images. Steformer (Lin et al., 2023a) designs a bi-branch Transformer-based structure to extract and integrate cross-view information from low-resolution stereo images. However, existing methods do not explore feature fusion in multi-scale space to improve low-resolution image recognition. In this paper, we propose a cascaded multi-scale attention mechanism that constructs enriched features in multi-scale spaces for low-resolution images.

2.3. CNN-ViT Hybrids

Hybrid models that combine convolutions and Vision Transformer (ViT) (Dosovitskiy et al., 2021) are gaining interest for their ability to capture fine-grained local details while preserving global dependency. To enhance fine-grained information, some methods apply the attention mechanisms to sub-regions or tokens within feature maps. Swin (Liu et al., 2021) employs shifted windows in the self-attention mechanism to capture both local and global information. CSwin (Dong et al., 2022) introduces a cross-shaped window to enhance the self-attention mechanism and further improve model capacity. NAT (Hassani et al., 2023) proposes a scalable sliding window attention mechanism by localizing self-attention to the nearest neighboring pixels. QFormer (Zhang et al., 2024) extends the window-based attention mechanism within adaptive quadrangles for learning better feature representation. With the demand for facilitating the aggregation of spatial information, many studies integrate convolutions within the attention mechanism. MobileViT (Mehta and Rastegari, 2022) and EfficientFormer (Li et al., 2022b) combine convolutions with Transformers to achieve efficient local and global feature extraction. CvT (Wu et al., 2021), IRMB (Zhang et al., 2023b) and SBCFormer (Lu et al., 2024) introduce depth-wise separable convolutions into the self-attention mechanism to improve representational power. Recent CNN-ViT hybrid methods demonstrate promising performance in high-resolution image recognition, but their accuracy is limited by the inherent challenges of low-resolution images. In this paper, we propose an effective hybrid network architecture tailored for low-resolution images.

3. Attention Mechanism for Low-Resolution Inputs

3.1. Motivation

In various tasks including pose estimation, it’s widely acknowledged that enabling multi-scale feature extraction and interaction between different scale features is crucial for achieving high-precision inference. In existing architectures, the multi-scale space is typically generated by simply downsampling the feature maps. However, this method poses a challenge when the input image resolution is low, as downsampling leads to a substantial reduction in the resolution of the resulting feature maps, leading to a considerable loss of information¹.

¹Regardless of the input resolution, stage-wise integration of spatial information via downsampling, which is fundamental to CNN-ViT hybrids, remains effective. The discussion above addresses a different aspect, focusing on the multi-scale feature processing *within* each processing stage in CNN-ViT hybrids.

To overcome this challenge, our study aims to devise an effective method for handling multi-scale feature maps without relying on downsampling. We approach this goal by enhancing the attention mechanism in CNN-ViT hybrids.

3.2. Basic Ideas: Cascaded Multi-Scale Attention (CMSA)

There are two primary ideas. The first involves directing each head of the multi-head self-attention mechanism to handle features from different scales. While conventional multi-head self-attention mechanisms already possess sufficient flexibility, they may not inherently fulfill this role. Contrarily, previous research has shown that attention maps tend to exhibit similarity between heads, leading to redundancy (Heo et al., 2021; Bolya et al., 2022; Chen et al., 2022).

To address this, we propose organizing the multi-heads into groups and implementing SwinT’s local window attention (Liu et al., 2021) within each group; see Figure 2c. We vary the window size for each group. This strategy aims to force different attention heads to effectively manage features of different scales. Our approach draws inspiration from the hybrid-scale attention (HSA) in SG-Former (Ren et al., 2023). However, HSA does not use SwinT’s local attention and instead adjusts key and value through token merging².

Our second idea involves implementing a new mechanism to enhance interaction among features of different scales across various groups. This entails organizing the groups in a specific order and transferring features obtained from local attention within one group to the next. These features are subsequently integrated into the attention computation within each group, resulting in an architecture that operates in a cascade-style fashion, as depicted in Figure 2c.

This approach draws inspiration from EfficientViT (Liu et al., 2023). It divides multi-head attention into groups and performs cascaded information integration, and our method follows the same principle. However, in EfficientViT, processing within groups primarily employs standard self-attention, and the scale of feature maps is the same across all groups. Its aim is to improve the trade-off between computational cost and expressive power. In contrast, our approach emphasizes fostering interactions between features of different scales. We also design a new method for integrating information between groups to achieve this goal.

3.3. Details of CMSA

We will now describe the cascaded multi-scale attention mechanism; see Figure 2c. Let \mathbf{X} be the input to our cascaded multi-scale attention mechanism; \mathbf{X} is a feature map with the size $H \times W \times C$. We first apply point-wise convolutions (PW-Conv) to \mathbf{X} to obtain $\mathbf{Q} \in \mathbb{R}^{H \times W \times D}$, $\mathbf{K} \in \mathbb{R}^{H \times W \times D}$, and $\mathbf{V} \in \mathbb{R}^{H \times W \times D}$.

We employ multi-head self-attention (MHSA), similar to the standard Transformer architecture. Specifically, \mathbf{Q} , \mathbf{K} , and \mathbf{V} are split (and reshaped) into $\tilde{\mathbf{Q}}_i$, $\tilde{\mathbf{K}}_i$, and $\tilde{\mathbf{V}}_i \in \mathbb{R}^{H \times W \times d_i}$

²While we initially experimented with the hybrid-scale attention mechanism, we found that our method based on local attention works much better.

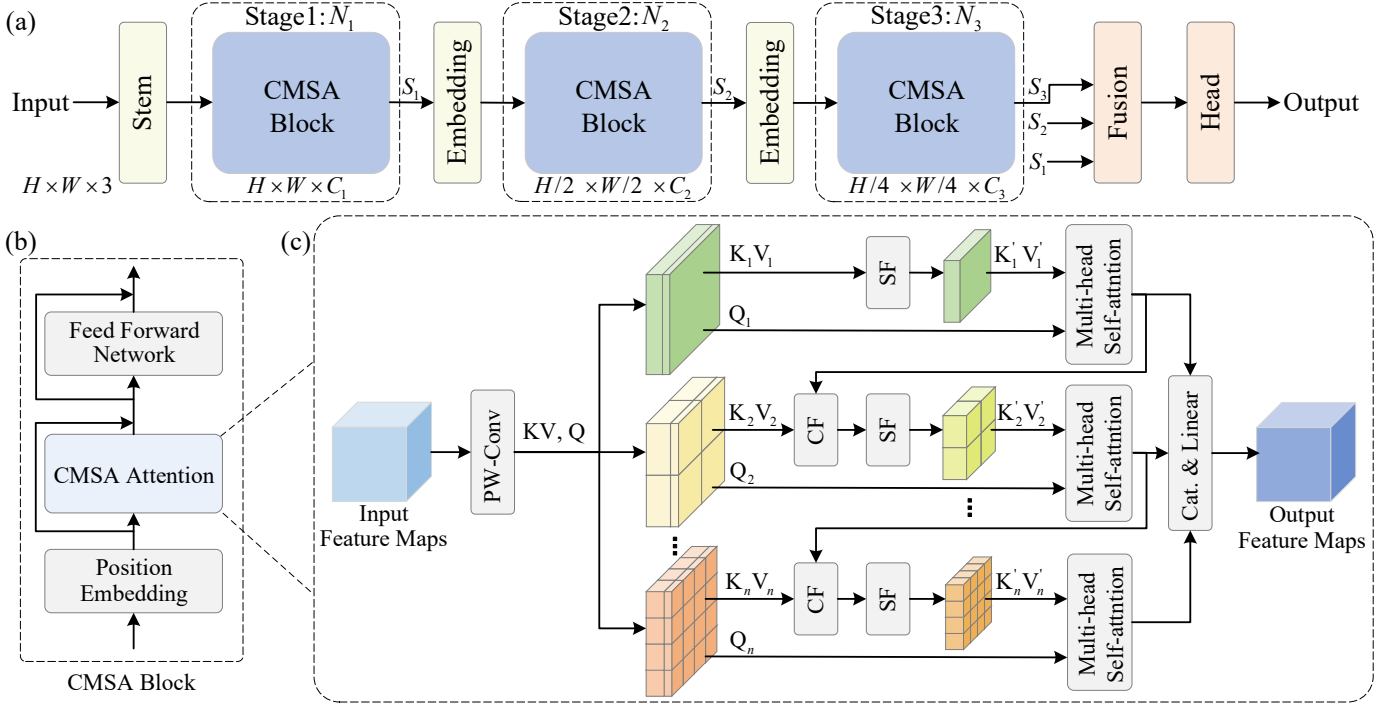


Fig. 2. Design of the proposed model. (a) The overall architecture. (b) Design of the basic blocks. (c) Proposed cascaded multi-scale attention (CMSA). See texts for details.

($i = 1, \dots, h$), where d_i is the feature dimension in this head. Then each head i conducts a self-attention computation as $\text{softmax}(\hat{\mathbf{Q}}_i \cdot \hat{\mathbf{K}}_i^T / \sqrt{d_i}) \cdot \hat{\mathbf{V}}_i$.

To deal with multi-scale features, we employ a group structure, as mentioned earlier. Specifically, we divide the heads into n groups, enabling each group to extract and foster features with different scales. Thus, \mathbf{Q} , \mathbf{K} , and \mathbf{V} are segmented in their channel dimensions to yield query, key, and value for each group as $\mathbf{K}_1, \dots, \mathbf{K}_n$, $\mathbf{Q}_1, \dots, \mathbf{Q}_n$, and $\mathbf{V}_1, \dots, \mathbf{V}_n$; $\mathbf{Q}_k, \mathbf{K}_k, \mathbf{V}_k \in \mathbb{R}^{H \times W \times d_k}$.

We employ SwinT’s local window attention in each group. Let the index of groups be $k = 1, \dots, n$. For the k -th group, we set the local window size to $s_k \times t_k$. Thus, the k -th group has $H/s_k \times W/t_k$ local windows, each with $s_k \times t_k$ size. We set $(s_1, t_1) = (H, W)$, meaning that the first head group ($k = 1$) extracts global features as the window size is the same as the input feature map (i.e., $H \times W$). The subsequent groups, with $s_k < H$ and $t_k < W$, extract local features with the specified window size $s_k \times t_k$.

To enable different scale features to interact with each other, we incorporate the cascaded structure of feature propagation and integration over the head groups, as explained above. Specifically, the k -th stream receives \mathbf{Q}_k , \mathbf{K}_k , and \mathbf{V}_k as inputs and outputs an updated feature map $\mathbf{X}'_k \in \mathbb{R}^{H \times W \times d_k}$ at its end. This output \mathbf{X}'_k is transferred to the intermediate section of the next (i.e., $(k + 1)$ -th) stream, contributing to the computation of the stream’s output \mathbf{X}'_{k+1} .

Specifically, the k -th group, starting with \mathbf{Q}_k , \mathbf{K}_k , and \mathbf{V}_k , receives the output \mathbf{X}'_{k-1} from the lower stream and updates \mathbf{K}_k and \mathbf{Q}_k as

$$\text{Concat}(\mathbf{K}'_k, \mathbf{V}'_k) = \text{SF}(\text{CF}(\text{Concat}(\mathbf{K}_k, \mathbf{V}_k, \mathbf{X}'_{k-1}))), \quad (1)$$

where Concat indicates the concatenation of \mathbf{K}_k , \mathbf{V}_k , and \mathbf{X}'_{k-1} in their channel dimension; CF (channel fusion) is a point-wise convolution, aiming to make its input exchange information in the channel dimension; on the other hand, SF (spatial fusion) aims at spatial exchange of information in the feature map. Specifically, it is implemented as a series of a depth-wise convolution with a 3×3 kernel, a GeLU activation function, and a point-wise convolution³. For the first stream with $k = 1$, it does not have a lower stream and thus \mathbf{K}'_1 and \mathbf{V}'_1 are computed as $\text{Concat}(\mathbf{K}'_1, \mathbf{V}'_1) = \text{SF}(\text{Concat}(\mathbf{K}_1, \mathbf{V}_1))$.

Then, the local attention with a window size $s_k \times t_k$ is computed between the query \mathbf{Q}_k and the updated key \mathbf{K}'_k and is applied to the updated value \mathbf{V}'_k , yielding the feature map \mathbf{X}'_k . Note that each group has multiple heads in each of which local, multi-head attention is computed. Finally, all the outputs from all the streams are aggregated to yield the output \mathbf{X}'' of the attention mechanism as

$$\mathbf{X}'' = \text{Linear}(\text{Concat}(\mathbf{X}'_1, \dots, \mathbf{X}'_n)), \quad (2)$$

where Linear is a linear transformation implemented as a linear layer with learnable weights.

Optional Setting of Attention. So far, we have considered the standard setting of attention where the query, key, and value all share the same dimensions. Prior studies (Graham et al., 2021; Wang et al., 2022b; Guo et al., 2022) demonstrate that making

³An optional average pooling with a 2×2 kernel to reduce the size of K and V .

Table 1. CMSA variants with different model sizes.

Stage	Output Size	Block	CMSA								
			S			B			L		
Stem	32×24	Patch Embed.	× 2 ($k = 3 \times 3$)								
			dim. 96			dim. 128			dim. 128		
1	32×24	CMSA Block	× 2			× 2			× 2		
			$n = 3$ groups			$n = 3$ groups			$n = 3$ groups		
			$s_1=32$	$s_2=16$	$s_3=8$	$s_1=32$	$s_2=16$	$s_3=8$	$s_1=32$	$s_2=16$	$s_3=8$
			$t_1=24$	$t_2=12$	$t_3=6$	$t_1=24$	$t_2=12$	$t_3=6$	$t_1=24$	$t_2=12$	$t_3=6$
			$d_1=32$	$d_2=32$	$d_3=16$	$d_1=16$	$d_2=32$	$d_3=16$	$d_1=16$	$d_2=32$	$d_3=16$
		$head=2$	$head=2$	$head=1$	$head=1$	$head=2$	$head=1$	$head=2$	$head=1$		
2	16×12	CMSA Block	× 1 ($k = 3 \times 3$)								
			dim. 160			dim. 192			dim. 256		
			× 4			× 4			× 4		
			$n = 2$ groups			$n = 2$ groups			$n = 2$ groups		
			$s_1=16$	$s_2=8$		$s_1=16$	$s_2=8$		$s_1=16$	$s_2=8$	
$t_1=12$	$t_2=6$		$t_1=12$	$t_2=6$		$t_1=12$	$t_2=6$				
$d_1=48$	$d_2=48$		$d_1=48$	$d_2=48$		$d_1=48$	$d_2=48$				
	$head=3$	$head=3$		$head=3$	$head=3$		$head=3$	$head=3$			
3	8×6	CMSA Block	× 1 ($k = 3 \times 3$)								
			dim. 224			dim. 256			dim. 320		
			× 3			× 3			× 3		
			$n = 2$ groups			$n = 2$ groups			$n = 2$ groups		
			$s_1=8$	$s_2=8$		$s_1=8$	$s_2=8$		$s_1=8$	$s_2=8$	
$t_1=6$	$t_2=6$		$t_1=6$	$t_2=6$		$t_1=6$	$t_2=6$				
$d_1=64$	$d_2=64$		$d_1=64$	$d_2=80$		$d_1=64$	$d_2=64$				
	$head=4$	$head=4$		$head=4$	$head=5$		$head=4$	$head=4$			

the key and value spatially smaller (or equivalently, using fewer tokens) than the query can enhance computational efficiency with the minimum sacrifice of inference accuracy. Specifically, we adjust the convolution in the spatial fusion (SF) module to halve the spatial dimensions of the key and value compared to the query, while doubling the channel size of the value relative to both the query and key. In our experiments, we employ this method to achieve a better trade-off of accuracy and computational cost.

3.4. Design of a Whole Network

3.4.1. Overall Design

We adopt a hierarchical pyramidal architecture, in line with recent CNN-ViT hybrids; see Figure 2a. The architecture starts with a ‘Stem’ block, followed by a sequence of stages. Each stage comprises multiple blocks that include the cascaded multi-scale attention mechanism explained above. A patch embedding layer is placed between stages to reduce the spatial resolution of feature maps.

The process begins with an input image of size $H \times W \times 3$, which is converted by the Stem into a feature map of dimensions $H \times W \times C$. With each subsequent stage, the resolution is halved, leading to feature map sizes of $H \times W$, $H/2 \times W/2$, and $H/4 \times W/4$, respectively. In the final stage, feature maps from each block are merged and funneled through a task-specific head component, resulting in the final output.

3.4.2. Design of a Block

As shown in Figure 2b, a single block consists of three components: position embedding, the cascaded multi-scale attention, and a feed-forward network.

For position embedding, we employ conditional positional embedding via depth-wise convolution.

$$\mathbf{X}_{PE} = PE(\mathbf{X}_{in}) \quad (3)$$

We choose 3×3 depth-wise convolution for PE. We incorporate a train-time overparametrization strategy (Chu et al., 2021; Vasu et al., 2023a), aiming at a better trade-off between inference accuracy and computational cost. Specifically, our network features three parallel branches in this section during the training phase: a 3×3 depth-wise convolution, a point-wise convolution, and batch normalization. These branches are reparametrized into a single depth-wise convolution at the testing phase. Following the depth-wise convolution, we utilize the GeLU activation function.

The resulting feature map is fed into the aforementioned cascaded multi-scale attention mechanism (CMAtn) with one residual connection as

$$\mathbf{X}_{attn} = \text{CMAtn}(\text{BN}(\mathbf{X}_{PE})) + \mathbf{X}_{PE}, \quad (4)$$

where BN denotes Batch Normalization. Its output is fed into a feed-forward network (FFN), following the standard design of ViTs (Dosovitskiy et al., 2021) as

$$\mathbf{X}_{out} = \text{FFN}(\text{LN}(\mathbf{X}_{attn})) + \mathbf{X}_{attn}, \quad (5)$$

Table 2. Results on bottom-up human pose estimation with the COCO 2017 val dataset. † means the values reported in the respective papers. * indicates models trained with a different learning rate scheduler.

Model	Backbone	Input Resolution	Params (M)	COCO 2017 val					
				AP↑	AP ⁵⁰	AP ⁷⁵	AP ^M	AP ^L	AR↑
SimpleBaseline [†] (Xiao et al., 2018)	ResNet-50	128 × 96	34.0	59.3	85.5	67.4	57.8	63.8	66.6
HRNet-W32 [†] (Sun et al., 2019)	HRNet-W32	128 × 96	28.5	66.9	88.7	76.3	64.6	72.3	73.7
HRNet-W48 [†] (Sun et al., 2019)	HRNet-W48	128 × 96	63.6	68.0	88.9	77.4	65.7	73.7	74.7
DARK [†] Zhang et al. (2020a)	HRNet-W32	128 × 96	28.5	70.7	88.9	78.4	67.9	76.6	76.7
UDP (Huang et al., 2020)	HRNet-W32	128 × 96	28.6	69.5	91.3	77.7	67.9	72.2	73.7
HRFormer-B (Yuan et al., 2021b)	HRFormer-B	128 × 96	43.0	66.2	88.2	76.1	64.1	71.8	73.0
ViTPose-B (Xu et al., 2022)	ViT-B	128 × 96	86.0	67.8	88.3	76.2	65.9	73.3	74.6
PCT-B (Geng et al., 2023)	Swin-B	128 × 96	87.0	66.4	90.5	75.7	65.1	68.7	70.1
CMSA-B	CMSA-B	128 × 96	5.6	70.3	91.3	77.8	67.9	77.4	74.6
CMSA-L	CMSA-L	128 × 96	7.3	71.5	91.4	79.2	69.0	75.4	75.5
HRNet-W32 (Sun et al., 2019)	HRNet-W32	64 × 48	28.5	58.3	86.2	67.1	57.4	62.3	66.2
CAL [†] (Wang et al., 2022a)	HRNet-W48	64 × 48	110.3	61.5	88.1	68.7	60.7	63.5	64.8
UDP (Huang et al., 2020)	HRNet-W32	64 × 48	28.6	62.8	86.4	70.9	61.3	67.8	70.4
HRFormer-B (Yuan et al., 2021b)	HRFormer-B	64 × 48	43.0	60.9	87.1	70.6	60.0	65.2	68.7
ViTPose-B (Xu et al., 2022)	ViT-B	64 × 48	86.0	63.8	86.5	72.6	62.5	68.7	71.4
PCT-B (Geng et al., 2023)	Swin-B	64 × 48	87.0	62.0	90.5	71.9	61.4	63.8	66.7
CMSA-B*	CMSA-B	64 × 48	5.6	64.7	87.6	72.3	62.9	69.7	71.7
CMSA-L*	CMSA-L	64 × 48	7.5	65.9	88.1	74.5	64.0	70.2	72.7
CMSA-B	CMSA-B	64 × 48	5.6	65.2	91.4	75.3	63.0	68.7	69.3
CMSA-L	CMSA-L	64 × 48	7.3	66.0	91.5	76.4	63.6	69.5	70.0
HRNet-W32 (Sun et al., 2019)	HRNet-W32	32 × 24	28.5	42.6	79.6	41.5	43.4	44.6	52.7
UDP (Huang et al., 2020)	HRNet-W32	32 × 24	28.6	51.9	81.7	56.8	51.5	55.9	61.4
HRFormer-B (Yuan et al., 2021b)	HRFormer-B	32 × 24	43.0	45.4	81.8	46.2	45.9	48.0	55.3
ViTPose-B (Xu et al., 2022)	ViT-B	32 × 24	86.0	51.2	81.0	56.1	50.7	55.0	60.4
PCT-B (Geng et al., 2023)	Swin-B	32 × 24	87.0	44.4	84.6	41.8	45.3	43.7	50.7
CMSA-S	CMSA-S	32 × 24	4.1	52.3	84.0	57.3	51.6	53.9	57.2
CMSA-B	CMSA-B	32 × 24	5.6	53.5	84.9	58.1	53.2	54.7	58.5
CMSA-L	CMSA-L	32 × 24	7.3	56.4	87.0	62.6	55.6	58.2	61.1

where LN denotes Layer Normalization. For the FNN, we employ a two-layer MLP with a GeLU activation function at its hidden layer.

The patch embedding layer comprises reparameterizable depth-wise and point-wise convolution layers, that use train-time overparameterization and these additional branches are removed by structural reparameterization at inference (Ding et al., 2021a,b).

3.4.3. Other Components

The Stem block and the patch embedding layers situated between the stages are each implemented as a convolutional layer. Specifically, we adopt a single pair consisting of a depth-wise convolution followed by a point-wise convolution for each, aiming to boost computational efficiency. For implementation, we adopt a train-time overparameterization strategy (Vasu et al., 2023b), similar to the one used for positional embedding, to achieve a favorable balance between accuracy and efficiency.

4. Experimental Results

We evaluate the effectiveness of our proposed method and compare it with existing models through experiments on three

distinct tasks: human pose estimation, head pose estimation, and small-image classification using CIFAR-10/100 datasets.

4.1. Human Pose Estimation

4.1.1. Dataset

We utilize the COCO 2017 dataset (Lin et al., 2014), comprising training, validation, and test sets with 118,000, 5,000, and 20,000 images, respectively. We adopt the bottom-up setting employed in many previous studies, in which the individual persons’ bounding boxes are provided⁴. Each person is labeled with 17 keypoints, and the models are tasked with predicting these keypoints’ coordinates based on the cropped and resized image from its bounding box in the input image. The dataset contains 250,000 individuals, with their heights in the original images ranging from 32 pixels to over 128 pixels throughout the dataset. These images are resized to a standard size before being fed into a model and we adjust this size to manipulate the input resolution.

⁴We use the official Github repository of HRNet (Sun et al., 2019) as a framework for the experiments: <https://github.com/leoxiaobin/deep-high-resolution-net.pytorch>.

Table 3. Results on landmark-free head pose estimation with the BIWI Fanelli et al. (2013) and AFLW2000 Zhu et al. (2016) datasets. Models are trained on the 300W-LP Zhu et al. (2016) dataset. † means the values reported in the respective papers.

Model	Input Resolution	Params (M)	BIWI				AFLW2000			
			Yaw	Pitch	Roll	MAE↓	Yaw	Pitch	Roll	MAE↓
Hopenet($\alpha=2$) † (Ruiz et al., 2018)	224×224	23.0	5.17	6.98	3.39	5.18	6.47	6.56	5.44	6.16
Shao † et al. (Shao et al., 2019)	224×224	24.6	4.59	7.25	6.15	6.00	5.07	6.37	4.99	5.48
WHENet † (Zhou and Gregson, 2020)	224×224	4.4	3.99	4.39	3.06	3.81	5.11	6.24	4.92	5.42
TokenHPE-v2 † (Zhang et al., 2023a)	224×224	85.9	3.95	4.51	2.71	3.72	4.36	5.54	4.08	4.66
QuatNet † (Hsu et al., 2019)	227×227	6.8	4.01	5.49	2.94	4.15	3.97	5.62	3.92	4.50
FDN † (Zhang et al., 2020b)	224×224	5.8	4.52	4.70	2.56	3.93	3.78	5.61	3.88	4.42
Li † et al. (Li et al., 2022a)	224×224	0.9	3.59	3.94	2.68	3.40	3.36	5.05	3.56	3.99
EVA-GCN † (Xin et al., 2021)	256×256	3.3	4.46	5.34	4.11	4.64	4.01	4.78	2.98	3.92
Li † et al. (Li et al., 2022a)	56×56	0.9	4.85	5.92	3.29	4.69	4.48	6.55	4.80	5.28
FSA-Net † (Yang et al., 2019)	64×64	5.1	4.27	4.96	2.76	4.00	4.50	6.08	4.64	5.07
TriNet † (Cao et al., 2021)	64×64	26.0	4.11	4.76	3.05	3.97	4.04	5.77	4.20	4.67
CMSA-B	64×64	5.4	4.47	5.29	3.15	4.30	4.08	5.30	4.06	4.48
CMSA-L	64×64	7.1	4.49	4.63	2.85	3.99	4.15	5.10	3.89	4.38
TriNet (Cao et al., 2021)	32×32	26.0	4.96	7.02	3.75	5.24	6.79	9.10	7.54	7.81
Li † et al. (Li et al., 2022a)	28×28	0.9	6.49	9.12	4.71	6.77	6.52	8.56	7.19	7.42
CMSA-S	32×32	4.0	4.81	4.85	3.24	4.33	4.01	5.65	4.12	4.59
CMSA-B	32×32	5.4	5.28	5.25	3.13	4.55	3.88	5.58	4.07	4.51
CMSA-L	32×32	7.1	4.97	5.36	3.12	4.48	3.84	5.54	3.99	4.46

4.1.2. Training

We consider the three variants with different model size, CMSA-S, -B, and -L, as shown in Table 1. We trained our CMSAs from scratch for 210 epochs using a mean squared error loss function, following the recipe from DeiT (Touvron et al., 2021), which is summarized as follows. We employed the AdamW (Loshchilov and Hutter, 2019) optimizer and applied a linear warm-up for the first five epochs. The initial learning rate was set to 2.5×10^{-3} , and the minimum value was set to 10^{-5} . The weight decay and momentum were set to 5×10^{-2} and 0.9, respectively, and a batch size of 32 was used. Data augmentation includes random rotation, random scale, flipping, and random erasing during training. For comparison, we consider several state-of-the-art methods. For them, we employ their official repositories⁵ to train and evaluate them using smaller-sized images, which are not tested in their respective papers.

4.1.3. Results

Table 2 presents the results at various input resolutions. Following prior studies, we employ the standard evaluation metrics based on object keypoint similarity (OKS) to gauge the accuracy of the models. Our CMSAs demonstrate superior performance across all tested resolutions, notably surpassing com-

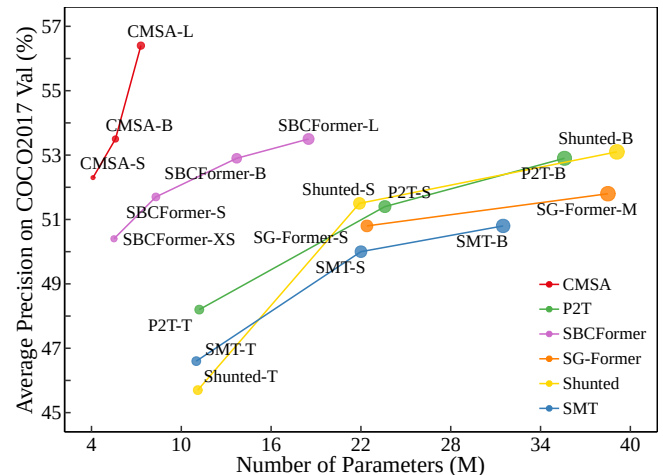


Fig. 3. Average Precision vs. Parameters. All models are trained for human pose estimation with input size 32×32 .

petitors by a wider margin at lower input resolutions⁶. This underscores our model’s efficacy in delivering high performance for low-resolution images.

Figure 3 presents the performance of methods using typical backbones with multi-scale representation for human pose estimation on 32×32 images. Our CMSAs consistently outperform the comparison methods, demonstrating superior multi-scale representation abilities on low-resolution images.

⁵UDP: <https://github.com/HuangJunJie2017/UDP-Pose>, HRFormer: <https://github.com/HRNet/HRFormer>, ViTPose: <https://github.com/ViTAE-Transformer/ViTPose>, PCT: <https://github.com/Gengzigang/PCT>, P2T: <https://github.com/yuhuan-wu/P2T>, SG-Former: <https://github.com/OliverRensu/SG-Former>, Shunted: <https://github.com/OliverRensu/Shunted-Transformer>, SMT: <https://github.com/AFeng-x/SMT>, SBCFormer: <https://github.com/xyongLu/SBCFormer>.

⁶It is noteworthy that they tend to show slightly lower AR scores, it is attributable to the choice of learning rate schedulers; when trained with the same step scheduler (StepLRScheduler in PyTorch) as others including ViT-B, the models (CMSA-B* and -L* in Table 2) yield superior AR scores.

4.2. Head Pose Estimation

4.2.1. Datasets

We apply our model to head pose estimation in a setting that does not rely on facial landmarks⁷. Models are tasked with predicting the pitch, roll, and yaw angles of a person’s head from an appropriately cropped image. Before inputted to the models, these images are resized to a standard resolution. We adjust this resolution to manage the size of the input images effectively. Building on prior research, we train our model and the SOTA models on the 300W-LP dataset and assess their performance using both the BIWI and AFLW2000 datasets. BIWI dataset has roughly 15,000 frames generated from RGB-D videos captured by a Kinect device for different subjects and head poses. 300W-LP dataset contains 61,225 images and further expanded 122,450 samples with flipping. Most of the faces in the BIWI dataset are small angles (yaw: $\pm 75^\circ$, pitch: $\pm 60^\circ$, roll: $\pm 50^\circ$), while 300W-LP extends the original 300-W dataset to a large pose ($[-90^\circ, 90^\circ]$). The AFLW2000 dataset is from the first 2,000 images of the AFLW dataset (Koestinger et al., 2011). Following the previous studies (Ruiz et al., 2018; Yang et al., 2019), we discard 31 images with angles outside of $[-99^\circ, 99^\circ]$ in the AFLW2000 dataset.

4.2.2. Training

During training, we applied binned classification and soft stage-wise regression to estimate head pose from a single RGB image, as in (Yang et al., 2019). Our method was trained for 100 epochs on the 300W-LP dataset following the recipe from DeiT. The training utilized AdamW optimizer with cosine learning rate scheduling and an initial learning rate 2.5×10^{-3} . Batch size is set to 96. During training and evaluation, all images are cropped around the face to include the whole head, resized to 32×32 , and normalized using the mean and standard deviation from ImageNet dataset (Deng et al., 2009).

4.2.3. Results

Table 3 shows the results of ours and the state-of-the-art methods, where the standard evaluation metric, the mean absolute error (MAE), is adopted. At low-resolution settings of 64×64 and 32×32 , our CMSAs can obtain state-of-the-art performance for the AFLW2000 dataset. Especially, CMSA-L achieves an MAE of 4.46 on 32×32 images from AFLW2000, surpassing the performance of most typical models for higher image resolutions. For low-resolution images from BIWI dataset, our CMSA-L consistently achieves state-of-the-art performance.

4.3. Image Classification with CIFAR-10/100

4.3.1. Training

We train our models from scratch for 300 epochs, following DeiT’s (Touvron et al., 2021) recipe, with the same data augmentation, cross-entropy loss function, and AdamW optimizer.

The initial learning rate was set to 2.5×10^{-3} , and the batch size was 128. For data augmentation, we apply conventional techniques such as random cropping, random horizontal flipping, mixup, random erasing, and label smoothing. We adhere to the original authors’ code when training other models. All models undergo training under uniform conditions with respect to the number of epochs and data augmentation strategies during both training and testing phases.

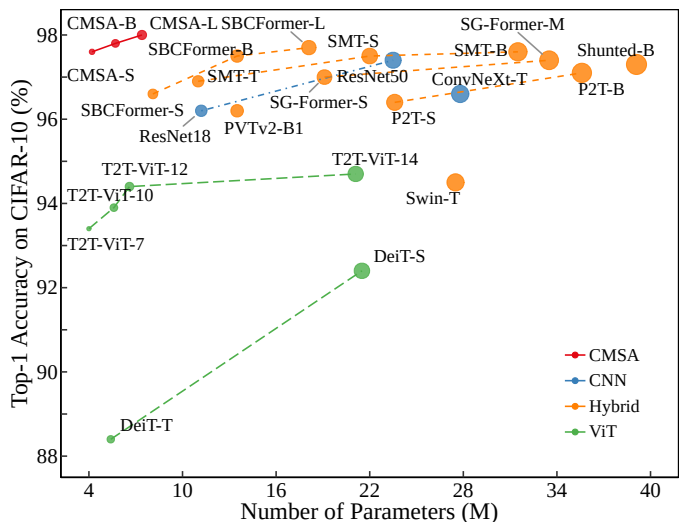


Fig. 4. Accuracy vs. Parameters. All models are trained for CIFAR-10 classification with input size 32×32 .

Table 4. Results on CIFAR-100 with input size 32×32 . † means the values reported in the respective papers.

Model	Params (M)	CIFAR-100 (%)
DeiT-B † (Touvron et al., 2021)	85.1	70.5
T2T-ViT _r -14 (Yuan et al., 2021a)	21.1	75.9
Swin-B † (Liu et al., 2021)	86.7	78.5
PVTv2-B1 (Wang et al., 2022b)	13.5	80.5
P2T-L (Wu et al., 2022)	53.9	81.8
ConvNeXt-B (Liu et al., 2022)	87.7	82.0
ResNet-50 (He et al., 2016)	23.5	82.9
SG-Former-M (Ren et al., 2023)	33.5	83.1
SMT-B (Lin et al., 2023b)	31.6	83.5
Shunted-B (Ren et al., 2022)	39.1	83.5
SG-Former-B (Ren et al., 2023)	77.1	83.8
SBCFormer-L (Lu et al., 2024)	18.2	84.1
CMSA-S	4.2	84.5
CMSA-B	5.7	85.0
CMSA-L	7.4	85.2

4.3.2. Results

Figure 4 and Table 4 present the performance of our models across varying parameter sizes compared to representative methods in CNNs, ViTs, and their hybrids. It shows averaged values over 300 trials. Notably, our largest model, CMSA-L,

⁷FSA-Net: <https://github.com/shamangary/FSA-Net>, TriNet: <https://github.com/anArkitek/TriNet.WACV2021>.

achieves 98.0% accuracy on CIFAR-10 and 85.2% accuracy on CIFAR-100, setting new benchmarks when limited to learning less than 300 epochs.

4.4. Ablation Study

The proposed CMSA can be decomposed into the following components: grouped multi-scale attention, cascaded feature propagation, spatial fusion (SF), and channel fusion (CF). To assess the effectiveness of each, we conduct an ablation test with human pose estimation using COCO 2017.

Table 5. Ablation tests of key components of CMSA for human pose estimation on COCO 2017 with 32×24 inputs.

Model	Standard Attn	Grouped Attn	Cascade	SF	CF	AP \uparrow
1	✓					48.3
2		✓				51.8
3		✓	✓			53.5
4		✓	✓	✓		54.4
5		✓	✓	✓	✓	56.4

Table 5 presents the results. The model in the first row, which has a hierarchical pyramid structure identical to our proposed network as shown in Figure 2a but uses standard self-attention instead of CMSA, performs the worst. The second-row model, while maintaining the same architecture, incorporates grouped multi-scale attention but lacks cascaded feature propagation, resulting in moderate performance improvements over the first model. The third-row model includes cascaded feature propagation but lacks other components, specifically removing CF and SF from the full model. The fourth-row model includes CF, and the fifth-row model includes both CF and SF, completing the network with CMSA. The performance improvements in these models demonstrate the effectiveness of the added components.

5. Conclusion

In this paper, we address the challenge of making visual inference on target objects from their low-resolution images, a critical issue in scenarios where targets are captured at low resolutions, such as with distant surveillance cameras or on low-performance edge devices. To mitigate the limitations inherent in low-resolution inputs—specifically, the difficulty in managing multi-scale features without compromising valuable information—we developed a novel attention mechanism, termed cascaded multi-scale attention (CMSA). This mechanism leverages a combination of multi-scale feature extraction and feature interactions, sidestepping the conventional downsampling operations for obtaining multi-scale features that typically result in loss of information in low-resolution contexts.

The empirical validation of our method across three tasks, i.e., human pose estimation, head pose estimation, and image classification, showed that our method surpasses current state-of-the-art approaches tailored to these applications, achieving

this with fewer parameters. These results underscore the potential of our proposed method to significantly improve image recognition tasks under constrained conditions, marking a step forward in the deployment of deep learning models on edge devices and in situations where only low-resolution images are available. In conclusion, our research contributes a useful framework for enhancing the accuracy of image recognition in less-than-ideal conditions where high-resolution data is not accessible.

Acknowledgments

References

- Bolya, D., Fu, C.Y., Dai, X., Zhang, P., Hoffman, J., 2022. Hydra attention: Efficient attention with many heads, in: European Conference on Computer Vision, Springer. pp. 35–49.
- Cao, Z., Chu, Z., Liu, D., Chen, Y., 2021. A vector-based representation to enhance head pose estimation, in: Proceedings of the IEEE/CVF Winter Conference on Applications of Computer Vision, pp. 1188–1197.
- Chen, C.F.R., Fan, Q., Panda, R., 2021. Crossvit: Cross-attention multi-scale vision transformer for image classification, in: Proceedings of the IEEE/CVF international conference on computer vision, pp. 357–366.
- Chen, T., Zhang, Z., Cheng, Y., Awadallah, A., Wang, Z., 2022. The principle of diversity: Training stronger vision transformers calls for reducing all levels of redundancy, in: Proceedings of the IEEE/CVF Conference on Computer Vision and Pattern Recognition, pp. 12020–12030.
- Cheng, B., Xiao, B., Wang, J., Shi, H., Huang, T.S., Zhang, L., 2020. High-erhnet: Scale-aware representation learning for bottom-up human pose estimation, in: Proceedings of the IEEE/CVF conference on computer vision and pattern recognition, pp. 5386–5395.
- Chu, X., Tian, Z., Zhang, B., Wang, X., Wei, X., Xia, H., Shen, C., 2021. Conditional positional encodings for vision transformers. arXiv preprint arXiv:2102.10882.
- Deng, J., Dong, W., Socher, R., Li, L.J., Li, K., Fei-Fei, L., 2009. Imagenet: A large-scale hierarchical image database, in: 2009 IEEE conference on computer vision and pattern recognition, Ieee. pp. 248–255.
- Ding, X., Zhang, X., Han, J., Ding, G., 2021a. Diverse branch block: Building a convolution as an inception-like unit, in: Proceedings of the IEEE/CVF Conference on Computer Vision and Pattern Recognition, pp. 10886–10895.
- Ding, X., Zhang, X., Ma, N., Han, J., Ding, G., Sun, J., 2021b. Repvgg: Making vgg-style convnets great again, in: Proceedings of the IEEE/CVF conference on computer vision and pattern recognition, pp. 13733–13742.
- Dong, X., Bao, J., Chen, D., Zhang, W., Yu, N., Yuan, L., Chen, D., Guo, B., 2022. Cswin transformer: A general vision transformer backbone with cross-shaped windows, in: Proceedings of the IEEE/CVF conference on computer vision and pattern recognition, pp. 12124–12134.
- Dosovitskiy, A., Beyer, L., Kolesnikov, A., Weissenborn, D., Zhai, X., Unterthiner, T., Dehghani, M., Minderer, M., Heigold, G., Gelly, S., Uszkoreit, J., Houlsby, N., 2021. An image is worth 16x16 words: Transformers for image recognition at scale, in: 9th International Conference on Learning Representations ICLR.
- Fanelli, G., Dantone, M., Gall, J., Fossati, A., Van Gool, L., 2013. Random forests for real time 3d face analysis. International journal of computer vision 101, 437–458.
- Geng, Z., Wang, C., Wei, Y., Liu, Z., Li, H., Hu, H., 2023. Human pose as compositional tokens, in: Proceedings of the IEEE/CVF Conference on Computer Vision and Pattern Recognition, pp. 660–671.
- Graham, B., El-Nouby, A., Touvron, H., Stock, P., Joulin, A., Jégou, H., Douze, M., 2021. Levit: a vision transformer in convnet’s clothing for faster inference, in: Proceedings of the IEEE/CVF international conference on computer vision, pp. 12259–12269.
- Guo, J., Han, K., Wu, H., Tang, Y., Chen, X., Wang, Y., Xu, C., 2022. Cmt: Convolutional neural networks meet vision transformers, in: Proceedings of the IEEE/CVF Conference on Computer Vision and Pattern Recognition, pp. 12175–12185.
- Hassani, A., Walton, S., Li, J., Li, S., Shi, H., 2023. Neighborhood attention transformer, in: Proceedings of the IEEE/CVF Conference on Computer Vision and Pattern Recognition, pp. 6185–6194.

- He, K., Zhang, X., Ren, S., Sun, J., 2016. Deep residual learning for image recognition, in: Proceedings of the IEEE conference on computer vision and pattern recognition, pp. 770–778.
- Heidari, M., Kazerouni, A., Soltany, M., Azad, R., Aghdam, E.K., Cohen-Adad, J., Merhof, D., 2023. Hiformer: Hierarchical multi-scale representations using transformers for medical image segmentation, in: Proceedings of the IEEE/CVF Winter Conference on Applications of Computer Vision, pp. 6202–6212.
- Heo, B., Yun, S., Han, D., Chun, S., Choe, J., Oh, S.J., 2021. Rethinking spatial dimensions of vision transformers, in: Proceedings of the IEEE/CVF International Conference on Computer Vision, pp. 11936–11945.
- Hsu, H.W., Wu, T.Y., Wan, S., Wong, W.H., Lee, C.Y., 2019. Quatnet: Quaternion-based head pose estimation with multiregression loss. *IEEE Transactions on Multimedia* 21, 1035–1046.
- Huang, J., Zhu, Z., Guo, F., Huang, G., 2020. The devil is in the details: Delving into unbiased data processing for human pose estimation, in: Proceedings of the IEEE/CVF conference on computer vision and pattern recognition, pp. 5700–5709.
- Huang, Z., Yang, S., Zhou, M., Li, Z., Gong, Z., Chen, Y., 2022. Feature map distillation of thin nets for low-resolution object recognition. *IEEE Transactions on Image Processing* 31, 1364–1379.
- Ibh, M., Grasshof, S., Witzner, D., Madeleine, P., 2023. Tempose: A new skeleton-based transformer model designed for fine-grained motion recognition in badminton, in: Proceedings of the IEEE/CVF Conference on Computer Vision and Pattern Recognition, pp. 5198–5207.
- Koestinger, M., Wohlhart, P., Roth, P.M., Bischof, H., 2011. Annotated facial landmarks in the wild: A large-scale, real-world database for facial landmark localization, in: 2011 IEEE international conference on computer vision workshops (ICCV workshops), IEEE. pp. 2144–2151.
- Li, X., Zhang, D., Li, M., Lee, D.J., 2022a. Accurate head pose estimation using image rectification and a lightweight convolutional neural network. *IEEE Transactions on Multimedia* .
- Li, Y., Hu, J., Wen, Y., Evangelidis, G., Salahi, K., Wang, Y., Tulyakov, S., Ren, J., 2022b. Rethinking vision transformers for mobilenet size and speed. *arXiv preprint arXiv:2212.08059* .
- Lin, J., Yin, L., Wang, Y., 2023a. Steformer: Efficient stereo image super-resolution with transformer. *IEEE Transactions on Multimedia* 25, 8396–8407.
- Lin, T.Y., Maire, M., Belongie, S., Hays, J., Perona, P., Ramanan, D., Dollár, P., Zitnick, C.L., 2014. Microsoft coco: Common objects in context, in: Computer Vision—ECCV 2014: 13th European Conference, Zurich, Switzerland, September 6–12, 2014, Proceedings, Part V 13, Springer. pp. 740–755.
- Lin, W., Wu, Z., Chen, J., Huang, J., Jin, L., 2023b. Scale-aware modulation meet transformer, in: Proceedings of the IEEE/CVF International Conference on Computer Vision, pp. 6015–6026.
- Liu, X., Peng, H., Zheng, N., Yang, Y., Hu, H., Yuan, Y., 2023. Efficientvit: Memory efficient vision transformer with cascaded group attention, in: Proceedings of the IEEE/CVF Conference on Computer Vision and Pattern Recognition (CVPR), pp. 14420–14430.
- Liu, Z., Lin, Y., Cao, Y., Hu, H., Wei, Y., Zhang, Z., Lin, S., Guo, B., 2021. Swin transformer: Hierarchical vision transformer using shifted windows, in: Proceedings of the IEEE/CVF international conference on computer vision, pp. 10012–10022.
- Liu, Z., Mao, H., Wu, C.Y., Feichtenhofer, C., Darrell, T., Xie, S., 2022. A convnet for the 2020s, in: Proceedings of the IEEE/CVF conference on computer vision and pattern recognition, pp. 11976–11986.
- Loshchilov, I., Hutter, F., 2019. Decoupled weight decay regularization, in: 7th International Conference on Learning Representations, ICLR.
- Lu, X., Suganuma, M., Okatani, T., 2024. Sbcformer: Lightweight network capable of full-size imagenet classification at 1 fps on single board computers, in: Proceedings of the IEEE/CVF Winter Conference on Applications of Computer Vision, pp. 1123–1133.
- Lu, Z., Li, J., Liu, H., Huang, C., Zhang, L., Zeng, T., 2022. Transformer for single image super-resolution, in: Proceedings of the IEEE/CVF conference on computer vision and pattern recognition, pp. 457–466.
- Mehta, S., Rastegari, M., 2022. Mobilevit: Light-weight, general-purpose, and mobile-friendly vision transformer, in: The Tenth International Conference on Learning Representations.
- Mei, Y., Fan, Y., Zhou, Y., 2021. Image super-resolution with non-local sparse attention, in: Proceedings of the IEEE/CVF Conference on Computer Vision and Pattern Recognition (CVPR), pp. 3517–3526.
- Ren, S., Yang, X., Liu, S., Wang, X., 2023. Sg-former: Self-guided transformer with evolving token reallocation, in: Proceedings of the IEEE/CVF International Conference on Computer Vision, pp. 6003–6014.
- Ren, S., Zhou, D., He, S., Feng, J., Wang, X., 2022. Shunted self-attention via multi-scale token aggregation, in: Proceedings of the IEEE/CVF conference on computer vision and pattern recognition, pp. 10853–10862.
- Ruiz, N., Chong, E., Rehg, J.M., 2018. Fine-grained head pose estimation without keypoints, in: Proceedings of the IEEE conference on computer vision and pattern recognition workshops, pp. 2074–2083.
- Shao, M., Sun, Z., Ozay, M., Okatani, T., 2019. Improving head pose estimation with a combined loss and bounding box margin adjustment, in: 2019 14th IEEE International Conference on Automatic Face & Gesture Recognition (FG 2019), IEEE. pp. 1–5.
- Singh, M., Nagpal, S., Singh, R., Vatsa, M., 2021. Derivenet for (very) low resolution image classification. *IEEE Transactions on Pattern Analysis and Machine Intelligence* 44, 6569–6577.
- Sun, K., Xiao, B., Liu, D., Wang, J., 2019. Deep high-resolution representation learning for human pose estimation, in: Proceedings of the IEEE/CVF conference on computer vision and pattern recognition, pp. 5693–5703.
- Touvron, H., Cord, M., Douze, M., Massa, F., Sablayrolles, A., Jégou, H., 2021. Training data-efficient image transformers & distillation through attention, in: International Conference on Machine Learning, PMLR. pp. 10347–10357.
- Vasu, P.K.A., Gabriel, J., Zhu, J., Tuzel, O., Ranjan, A., 2023a. Fastvit: A fast hybrid vision transformer using structural reparameterization. *arXiv preprint arXiv:2303.14189* .
- Vasu, P.K.A., Gabriel, J., Zhu, J., Tuzel, O., Ranjan, A., 2023b. Mobileone: An improved one millisecond mobile backbone, in: Proceedings of the IEEE/CVF Conference on Computer Vision and Pattern Recognition, pp. 7907–7917.
- Wang, C., Zhang, F., Zhu, X., Ge, S.S., 2022a. Low-resolution human pose estimation. *Pattern Recognition* 126, 108579.
- Wang, W., Xie, E., Li, X., Fan, D.P., Song, K., Liang, D., Lu, T., Luo, P., Shao, L., 2021. Pyramid vision transformer: A versatile backbone for dense prediction without convolutions, in: Proceedings of the IEEE/CVF international conference on computer vision, pp. 568–578.
- Wang, W., Xie, E., Li, X., Fan, D.P., Song, K., Liang, D., Lu, T., Luo, P., Shao, L., 2022b. Pvt v2: Improved baselines with pyramid vision transformer. *Computational Visual Media* 8, 415–424.
- Wang, Y., Li, M., Cai, H., Chen, W.M., Han, S., 2022c. Lite pose: Efficient architecture design for 2d human pose estimation, in: Proceedings of the IEEE/CVF Conference on Computer Vision and Pattern Recognition, pp. 13126–13136.
- Wu, H., Xiao, B., Codella, N., Liu, M., Dai, X., Yuan, L., Zhang, L., 2021. Cvt: Introducing convolutions to vision transformers, in: Proceedings of the IEEE/CVF International Conference on Computer Vision, pp. 22–31.
- Wu, Y.H., Liu, Y., Zhan, X., Cheng, M.M., 2022. P2t: Pyramid pooling transformer for scene understanding. *IEEE transactions on pattern analysis and machine intelligence* 45, 12760–12771.
- Xiao, B., Wu, H., Wei, Y., 2018. Simple baselines for human pose estimation and tracking, in: Proceedings of the European conference on computer vision (ECCV), pp. 466–481.
- Xin, M., Mo, S., Lin, Y., 2021. Eva-gcn: Head pose estimation based on graph convolutional networks, in: Proceedings of the IEEE/CVF Conference on computer vision and pattern recognition, pp. 1462–1471.
- Xu, Y., Zhang, J., Zhang, Q., Tao, D., 2022. Vitpose: Simple vision transformer baselines for human pose estimation. *Advances in Neural Information Processing Systems* 35, 38571–38584.
- Yang, T.Y., Chen, Y.T., Lin, Y.Y., Chuang, Y.Y., 2019. Fsa-net: Learning fine-grained structure aggregation for head pose estimation from a single image, in: Proceedings of the IEEE/CVF Conference on Computer Vision and Pattern Recognition, pp. 1087–1096.
- Yu, C., Xiao, B., Gao, C., Yuan, L., Zhang, L., Sang, N., Wang, J., 2021. Lite-hrnet: A lightweight high-resolution network, in: Proceedings of the IEEE/CVF conference on computer vision and pattern recognition, pp. 10440–10450.
- Yuan, L., Chen, Y., Wang, T., Yu, W., Shi, Y., Jiang, Z.H., Tay, F.E., Feng, J., Yan, S., 2021a. Tokens-to-token vit: Training vision transformers from scratch on imagenet, in: Proceedings of the IEEE/CVF international conference on computer vision, pp. 558–567.
- Yuan, Y., Fu, R., Huang, L., Lin, W., Zhang, C., Chen, X., Wang, J., 2021b. Hrformer: High-resolution vision transformer for dense predict. *Advances in Neural Information Processing Systems* 34, 7281–7293.

- Zhang, C., Liu, H., Deng, Y., Xie, B., Li, Y., 2023a. Tokenhpe: Learning orientation tokens for efficient head pose estimation via transformers, in: Proceedings of the IEEE/CVF Conference on Computer Vision and Pattern Recognition, pp. 8897–8906.
- Zhang, F., Zhu, X., Dai, H., Ye, M., Zhu, C., 2020a. Distribution-aware coordinate representation for human pose estimation, in: Proceedings of the IEEE/CVF conference on computer vision and pattern recognition, pp. 7093–7102.
- Zhang, H., Wang, M., Liu, Y., Yuan, Y., 2020b. Fdn: Feature decoupling network for head pose estimation, in: Proceedings of the AAAI conference on artificial intelligence, pp. 12789–12796.
- Zhang, J., Li, X., Li, J., Liu, L., Xue, Z., Zhang, B., Jiang, Z., Huang, T., Wang, Y., Wang, C., 2023b. Rethinking mobile block for efficient neural models. arXiv preprint arXiv:2301.01146 .
- Zhang, M., Zhang, C., Zhang, Q., Guo, J., Gao, X., Zhang, J., 2023c. Es-saformer: Efficient transformer for hyperspectral image super-resolution, in: Proceedings of the IEEE/CVF International Conference on Computer Vision, pp. 23073–23084.
- Zhang, Q., Zhang, J., Xu, Y., Tao, D., 2024. Vision transformer with quadrangle attention. *IEEE Transactions on Pattern Analysis and Machine Intelligence* .
- Zhang, W., Huang, Z., Luo, G., Chen, T., Wang, X., Liu, W., Yu, G., Shen, C., 2022. Topformer: Token pyramid transformer for mobile semantic segmentation, in: Proceedings of the IEEE/CVF Conference on Computer Vision and Pattern Recognition, pp. 12083–12093.
- Zhou, Y., Gregson, J., 2020. Whenet: Real-time fine-grained estimation for wide range head pose, in: 31st British Machine Vision Conference 2020, BMVC 2020, Virtual Event, UK, September 7-10, 2020.
- Zhu, X., Lei, Z., Liu, X., Shi, H., Li, S.Z., 2016. Face alignment across large poses: A 3d solution, in: Proceedings of the IEEE conference on computer vision and pattern recognition, pp. 146–155.